

We are IntechOpen, the world's leading publisher of Open Access books Built by scientists, for scientists

6,900

Open access books available

186,000

International authors and editors

200M

Downloads

Our authors are among the

154

Countries delivered to

TOP 1%

most cited scientists

12.2%

Contributors from top 500 universities



WEB OF SCIENCE™

Selection of our books indexed in the Book Citation Index
in Web of Science™ Core Collection (BKCI)

Interested in publishing with us?
Contact book.department@intechopen.com

Numbers displayed above are based on latest data collected.
For more information visit www.intechopen.com



Application of Quaternary AlInGaN- Based Alloys for Light Emission Devices

Sara C. P. Rodrigues¹, Guilherme M. Sipahi², Luísa Scolfaro³
and Eronides F. da Silva Jr.⁴

¹*Departamento de Física - Universidade Federal Rural de Pernambuco*

²*Instituto de Física de São Carlos - Universidade de São Paulo*

³*Department of Physics - Texas State University*

⁴*Departamento de Física - Universidade Federal de Pernambuco*

^{1,2,4}Brazil

³USA

1. Introduction

Excellent progress has been made during the past few years in the growth of III-nitride materials and devices. Today, one of the most important application of novel optoelectronic devices is the design and engineering of light-emitting diodes (LEDs) working from ultraviolet (UV) through infrared (IR), thus covering the whole visible spectrum. Since the pioneer works of Nakamura *et al.* at Nichia Corporation in 1993 (Nakamura *et al.* (1995)) when the blue LEDs and pure green LEDs were invented, an enormous progress in this field was observed which has been reviewed by several authors (Ambacher (1998); Nakamura *et al.* (2000)). The rapid advances in the hetero-epitaxy of the group-III nitrides (Fernández-Garrido *et al.* (2008); Kemper *et al.* (2011); Suihkonen *et al.* (2008)) have facilitated the production of new devices, including blue and UV LEDs and lasers, high temperature and high power electronics, visible-blind photodetectors and field-emitter structures (Hirayama (2005); Hirayama *et al.* (2010); Tschumak *et al.* (2010); Xie *et al.* (2007); Zhu *et al.* (2007)).

There has been recent interest in the $\text{Al}_x\text{In}_{1-x-y}\text{Ga}_y\text{N}$ quaternary alloys due to potential application in UV LEDs and UV-blue laser diodes (LDs) once they present high brightness, high quantum efficiency, high flexibility, long-lifetime, and low power consumption (Fu *et al.* (2011); Hirayama (2005); Kim *et al.* (2003); Knauer *et al.* (2008); Liu *et al.* (2011); Park *et al.* (2008); Zhmakin (2011); Zhu *et al.* (2007)). The availability of the quaternary alloy offers an extra degree of freedom which allows the independent control of the band gap and lattice constant. Another interesting feature of the AlGaInN alloy is that it gives rise to higher emission intensities than the ternary AlGaInN alloy with the absence of In (Hirayama (2005); Wang *et al.* (2007)). An important issue is related to white light emission, which can be obtained by mixing emissions in different wavelengths with appropriate intensities (Roberts (1997); Rodrigues *et al.* (2007); Xiao *et al.* (2004)).

Highly conductive *p*-type III-nitride layers are of crucial importance, in particular, for the production of LEDs. Although the control of *p*-doping in these materials is still subject of discussion, remarkable progress has been achieved (Hirayama (2005); Zhang *et al.* (2011)) and

recently reported experimental results point towards acceptor doping concentration high as $\approx 10^{19} \text{ cm}^{-3}$ (Liu et al. (2011); Zado et al. (2011); Zhang et al. (2011)).

The group-III nitrides crystallize in both, the stable wurtzite (w) phase and the metastable cubic (c) phase. Unlike for the hexagonal w-structure, the growth of cubic GaN is more complicated due to the thermodynamically unstable nature of the structure. In hexagonal GaN inherent spontaneous and piezoelectric polarization fields are present along the c-axis because of the crystal symmetry. Due to these fields, non-polar and semi-polar systems have attracted interest. One method to produce real non-polar materials is the growth of the c-phase. Considerable advances in the growth of c-nitrides, with the aim of getting a complete understanding of the c-nitride-derived heterostructures have been observed (As (2009); Schörmann et al. (2007)). Successful growth of quaternary c- $\text{Al}_x\text{In}_{1-x-y}\text{Ga}_y\text{N}$ layers lattice matched to GaN has been reported (Kemper et al. (2011); Schörmann et al. (2006)). The absence of polarization fields in the c-III nitrides may be advantageous for some device applications. Besides, it has been shown that these quaternary alloys can be doped easily as p-type, and due to the wavelength localization the optical transition energies are higher in the alloys than in GaN (Wang et al. (2007)).

However, the exact nature of the optical processes involved in the alloys with In is a subject of controversy. Different mechanisms have been proposed for the origin of the carriers' localized states in the quantum well devices. One is related to the low solubility of InN in GaN, leading to the presence of nanoclusters inside the alloy, which can be suppressed by biaxial strain as predicted and measured in c-InGaN samples (Marques et al. (2003); Scolfaro et al. (2004); Tabata et al. (2002)). The second mechanism proposes that the recombination occurs through the quantum confined states (electron-hole pairs or excitons) inside the well.

In this chapter we show the results of detailed studies of the theoretical photoluminescence (PL) and absorption spectra for several systems based on nitride quaternary alloys, using the $\vec{k} \cdot \vec{p}$ theory within the framework of effective mass approximation, in conjunction with the Poisson equation for the charge distribution. Exchange-correlation effects are also included within the local density approximation (Rodrigues et al. (2002); Sipahi et al. (1998)). All systems are assumed to be strained, so that the optical transitions are due to confinement effects. The theoretical method will be described in section 2. Through these calculations the possibility of obtaining light emission from undoped (see section 3) and p-doped (see section 4) quaternary $\text{Al}_X\text{In}_{1-X-Y}\text{Ga}_Y\text{N}/\text{Al}_x\text{In}_{1-x-y}\text{Ga}_y\text{N}$ superlattices (SLs) is addressed. By properly choosing the x and y contents in the wells and the acceptor doping concentration N_A as well X and Y in the barriers, it is shown to be possible to achieve light emission which covers the visible spectrum from violet to red. The investigation is also extended to double quantum wells (DQWs), as described in section 5, confronting the results with experimental data reported on these systems (Kyono et al. (2006)). The results are compared with regard to the PL emissions for the different systems, also when an external electric field is present. Finally it is shown that by adopting appropriated combinations of SLs is possible to obtain the best conditions in order to get white-light emission. This fact is fundamental in the design of new optoelectronic devices.

2. Theoretical band structure and luminescence spectra calculations

During the last few years, the super-cell $\vec{k} \cdot \vec{p}$ method has been adapted to quantum wells and superlattices (SLs) (Rodrigues et al. (2002); Sipahi et al. (1996)). Using this approach, one can self-consistently solve the 8×8 Kane multiband effective mass equation (EME) for the charge

distribution (Sipahi et al. (1998)). The results below are calculated assuming an infinite SL of squared wells along <001> direction.

The multiband EME is represented with respect to plane waves with vectors $K=(2\pi/d)l$ (l being an integer and d the SL period) equal to the reciprocal SL vector. The rows and columns of the 8×8 Kane Hamiltonian refer to the Bloch-type eigenfunctions $|jm_j\vec{k}\rangle$ of Γ_8 heavy- and light-hole bands, Γ_7 spin-orbit-split-hole band and Γ_6 conduction band; \vec{k} denotes a vector in the first SL Brillouin zone (BZ).

By expanding the EME with respect to plane waves ($z|K$) one is able to represent this equation with respect to Bloch functions ($\vec{r}|jm_j\vec{k} + K\vec{z}$). For a Bloch-type eigenfunction ($z|E\vec{k}$) of the SL of energy E and wavevector \vec{k} , the EME takes the form:

$$\sum_{j'm'_jK'} \left(jm_j\vec{k}K | H_0 + H_{ST} + V_{HET} + V_A + V_H + V_{XC} | j'm'_j\vec{k}K' \right) \left(j'm'_j\vec{k}K' | E\vec{k} \right) = E(\vec{k}) \left(jm_j\vec{k}K | E\vec{k} \right), \quad (1)$$

where H_0 is the effective kinetic energy operator, generalized for a heterostructures H_{ST} is the strain operator originated from the lattice mismatch, V_{HET} is the potential that arises from the band offset at the interfaces, which is diagonal with respect to $jm_j, j'm'_j$, V_{XC} is the exchange-correlation potential for carriers taken within Local Density Approximation (LDA), V_A is the ionized acceptor charge distribution potential, and V_H is the Hartree potential or one-particle potential felt by the carrier from the carriers charge density. So the Coulomb potential, V_C given by contribution of V_A and V_H potentials, can be obtained by means of the self-consistent procedure, where the Poisson equation stands, in the reciprocal space as,

$$(K | V_C | K') = \frac{4\pi e^2}{\epsilon} \frac{1}{|K - K'|^2} [(K | N_A(z) | K') - (K | p(z) | K')], \quad (2)$$

with ϵ being the dielectric constant, e the electron charge, $N_A(z)$ the ionized acceptors concentration, and $p(z)$ being the holes charge distribution, which is given by

$$p(z) = \sum_{\substack{jm_j\vec{k} \in \\ \text{empty states}}} |(zs | jm_j\vec{k})|^2, \quad (3)$$

where s is the spin coordinate.

The next term in the Hamiltonian is the strain potential, V_{ST} . The kind of strain in these systems is biaxial, so it can be decomposed into two terms, a hydrostatic term and an uniaxial term (Rodrigues et al. (2001)). Since the hydrostatic term changes the gap energy, thus not affecting the valence band potential depth, only the uniaxial strain component will be considered (Rodrigues et al. (2001)). This latter may be calculated by the following expression:

$$\epsilon = -2/3D_u\epsilon_{xx}(1 + 2C_{12}/C_{11}), \quad (4)$$

where $-2/3D_u$ is the shear deformation potential, C_{11} and C_{12} are the elastic constants, and ϵ_{xx} is the lattice mismatch which is given by:

$$\epsilon_{xx} = (a_{\text{barrier}} - a_{\text{well}})/a_{\text{well}}, \quad (5)$$

with $a_{barrier}$ and a_{well} being the lattice parameters of the barrier and well materials, respectively.

Through these definitions one can calculate the Fourier coefficients of the strain operator $(K|\epsilon(z)|K')$ and express the strain term of the Hamiltonian V_{ST} as follows:

$$(jm_j\vec{k}K|H_{ST}|j'm'_j\vec{k}K') = (K|\epsilon(z)|K')M_{jm_j}^{j'm'_j}, \quad (6)$$

where $M_{jm_j}^{j'm'_j}$ is defined as

$$M_{jm_j}^{j'm'_j} = \begin{pmatrix} 1 & 0 & 0 & 0 & 0 & 0 \\ 0 & -1 & 0 & 0 & -i\sqrt{2} & 0 \\ 0 & 0 & -1 & 0 & 0 & -i\sqrt{2} \\ 0 & 0 & 0 & 1 & 0 & 0 \\ 0 & i\sqrt{2} & 0 & 0 & 0 & 0 \\ 0 & 0 & i\sqrt{2} & 0 & 0 & 0 \end{pmatrix}. \quad (7)$$

Exchange-correlation effects can be taken into account in the local density approximation, by adopting a parameterized expression for an inhomogeneous hole gas, applying the exchange interaction only for identical particles and the correlation for all of them (Enderlein et al. (1997)). The band shift potential V_{HET} is diagonal with respect to $jm_j, j'm'_j$, and is defined by

$$(jm_j\vec{k}K|V_{HET}|j'm'_j\vec{k}K') = (K|V_{HET}|K')\delta_{jj'}\delta_{m_jm'_j} \quad (8)$$

where $(K|V_{HET}|K')$ are the Fourier coefficients of V_{HET} along the growth direction.

From the calculated eigenstates, one can determine the luminescence and absorption spectra of the SL by using the following general expression (Sipahi et al. (1998))

$$I(\omega) = \frac{2\hbar\omega^3}{c} \frac{e^2}{m_0c^2} \sum_{\vec{k}} \sum_{n_e} \sum_{\substack{n_q \\ q=hh, lh, so}} f_{n_en_q}(\vec{k}) N_{n_e\vec{k}} [1 - N_{n_q\vec{k}}] \times \frac{\gamma}{\pi [E_{n_e}(\vec{k}) - E_{n_q}(\vec{k}) - \hbar\omega]^2 + \gamma^2}, \quad (9)$$

where m_0 is the electron mass, ω is the incident radiation frequency, γ is the emission broadening (assumed as constant and equal to 10 meV), E_{n_e} and E_{n_q} are the energies associated to n_e and n_q , respectively, the electron and hole states involved in the transition. The occupation functions $N_{n_e\vec{k}}$ and $[1 - N_{n_q\vec{k}}]$ are the Fermi-like occupation functions for states in the conduction- and valence-band, respectively.

For the calculation of luminescence (absorption) spectra, the sum in Eq. (9) is performed over the occupied states in the conduction (valence) band, and unoccupied states in the valence (conduction) band (Sipahi et al. (1998)).

The oscillator strength, $f_{n_en_q}(\vec{k})$, is given by

$$f_{n_en_q}(\vec{k}) = \frac{2}{m_0} \sum_{\sigma_e\sigma_q} \frac{|\langle n_e\sigma_e\vec{k} | p_x | n_q\sigma_q\vec{k} \rangle|^2}{E_{n_e}(\vec{k}) - E_{n_q}(\vec{k})}, \quad (10)$$

	GaN	InN	AlN
γ_1	2.96	3.77	1.54
γ_2	0.90	1.33	0.42
γ_3	1.20	1.60	0.64
$\Delta_{so}(\text{meV})$	17	3	19
$a(\text{\AA})$	4.552	5.030	4.380
m_{hh}^*	0.86	0.84	1.44
m_{lh}^*	0.21	0.16	0.42
m_{so}^*	0.30	0.24	0.63
m_e^*	0.15	0.10	0.067
E_g^Γ (eV)	3.3	0.9	5.94
a_g (eV)	-8.50	-12.98	-9.40
$2/3D_u$ (eV)	1.6	1.2	1.5
C_{11} (GPa)	293	187	304
C_{12} (GPa)	159	125	160

Table 1. Values of the parameters used in the self-consistent calculations of the *p*-doped cubic $(\text{Al}_{0.20}\text{In}_{0.05}\text{Ga}_{0.75})\text{N}/(\text{Al}_x\text{In}_{1-x-y}\text{Ga}_y)\text{N}$ SLs. Data extracted from Refs. (Ramos et al. (2001); Rodrigues et al. (2000; 2002); Schörmann et al. (2006)).

where p_x is the dipole momentum in the *x*-direction, σ_e and σ_q denote the spin values for electron and holes, respectively.

All the parameters used in this analysis are shown in Table I. For the quaternary $(\text{Al}_x\text{In}_{1-x-y}\text{Ga}_y)\text{N}$ band gap energy dependence on the alloy contents, *x* and *y*, was used the expression provided in Ref. (Marques et al. (2003)). For all the other quantities, linear interpolations were taken using the values for the binaries, AlN, GaN, InN. The temperature dependence of bandgap energies was evaluated through the Varshni analytical expression as applied for GaN (Kohler et al. (2002)).

3. Undoped cubic $\text{Al}_x\text{In}_y\text{Ga}_{1-x-y}\text{N}$ systems

In order to analyze the effects of the use of quaternary alloys in the electronic transitions, Fig. 1 presents the theoretical PL spectra at $T = 2$ K calculated for strained undoped $\text{In}_{0.2}\text{Ga}_{0.8}\text{N}/\text{Al}_x\text{Ga}_y\text{In}_{1-x-y}\text{N}$ SLs with $x = 0.03, 0.10,$ and 0.20 and $y = 0.40, 0.47,$ and 0.51 , respectively. The barriers, constituted by the ternary alloy, have width $d_1 = 60$ nm, while the wells have width $d_2 = 3$ nm. It is important to remark that all systems are strained, so the luminescence cannot arise from nanoclusters created during the growth. In all cases in this section the first peak seen in the PL spectra corresponds to the first electronic transition E1-HH1 (first electron level E1 and first heavy-hole level HH1) (Rodrigues et al. (2005)).

From Fig. 1 one can observe that with the appropriate choice of parameters it is possible to reach wavelengths from the red to the blue region. One can also see that, by changing the well width as depicted in Fig. 2, the peaks in the PL spectra exhibit larger variations. As the well width decreases, the transition energy gets closer to the red region. This occurs because of the changes in the energies caused by the confinement and strain effects, which become stronger as the In content increases.

As the results described above are from systems where InGaN represents the barriers and the quaternary alloy is in the wells, one can change the picture and start analyzing systems where the barriers correspond to the quaternary alloys while the InGaN alloy forms the wells.

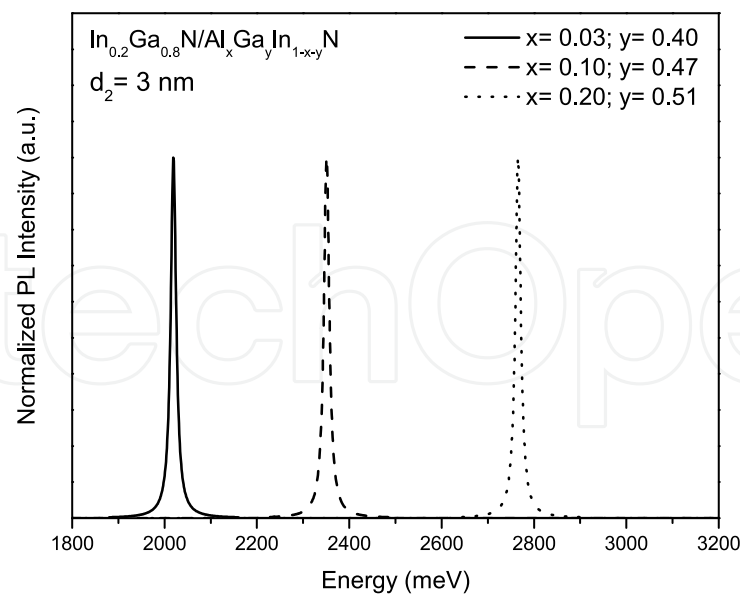


Fig. 1. Theoretical normalized PL spectra for strained undoped $\text{In}_{0.2}\text{Ga}_{0.8}\text{N}/\text{Al}_x\text{Ga}_y\text{In}_{1-x-y}\text{N}$ SLs, with $x=0.03$ (solid line), 0.10 (dashed line), and 0.20 (dotted line) and $y=0.40, 0.47$, and 0.51 , respectively, barrier width $d_1 = 60$ nm, well width $d_2 = 3$ nm.

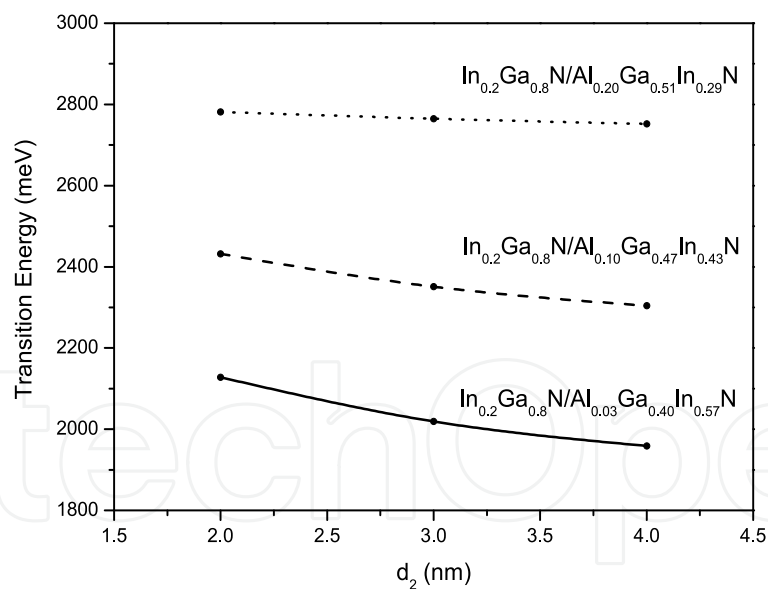


Fig. 2. PL peaks as a function of the well width d_2 for the same systems of Fig. 1.

Fig. 3 presents calculated SL systems with the same configurations as Fig. 1, but using GaN as barriers instead of $\text{Al}_x\text{Ga}_y\text{In}_{1-x-y}\text{N}$. It presents calculated theoretical PL spectra, at $T = 2$ K, for $\text{Al}_{0.10}\text{Ga}_{0.47}\text{In}_{0.43}\text{N}/\text{In}_{0.55}\text{Ga}_{0.45}\text{N}$, $\text{Al}_{0.17}\text{Ga}_{0.47}\text{In}_{0.36}\text{N}/\text{In}_{0.42}\text{Ga}_{0.68}\text{N}$, and $\text{Al}_{0.25}\text{Ga}_{0.47}\text{In}_{0.28}\text{N}/\text{In}_{0.25}\text{Ga}_{0.75}\text{N}$ SLs (solid lines). The figure presents also, for comparison, the systems of Fig. 1 (dashed lines). A similar behavior, as obtained in Fig.1, is seen also for InGaN barriers, with the possibility of light emission covering the entire visible spectra.

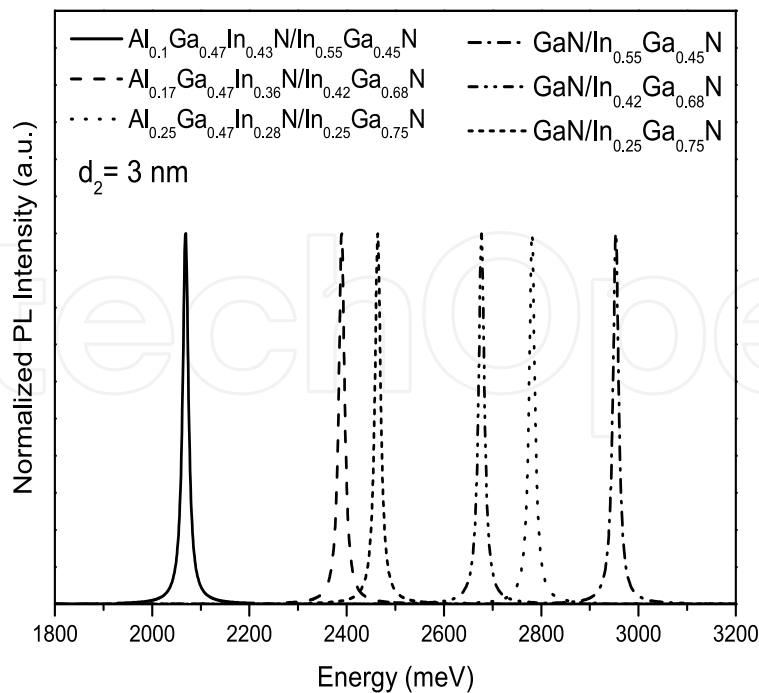


Fig. 3. Theoretical normalized PL spectra for the strained undoped SLs $\text{Al}_{0.10}\text{Ga}_{0.47}\text{In}_{0.43}\text{N}/\text{In}_{0.55}\text{Ga}_{0.45}\text{N}$ (solid line), $\text{Al}_{0.17}\text{Ga}_{0.47}\text{In}_{0.36}\text{N}/\text{In}_{0.42}\text{Ga}_{0.68}\text{N}$ (dashed line) and $\text{Al}_{0.25}\text{Ga}_{0.47}\text{In}_{0.28}\text{N}/\text{In}_{0.25}\text{Ga}_{0.75}\text{N}$ (dotted line). The barrier width is $d_1 = 60$ nm and the well width is $d_2 = 3$ nm. For comparison, we show the results for the SLs $\text{GaN}/\text{In}_{0.55}\text{Ga}_{0.45}\text{N}$ (dash-dotted line), $\text{GaN}/\text{In}_{0.42}\text{Ga}_{0.68}\text{N}$ (dash-dot-dotted line), and $\text{GaN}/\text{In}_{0.25}\text{Ga}_{0.75}\text{N}$ (short-dashed line) systems.

However, this is not possible using GaN in the barriers, since we have a limitation imposed by the fixed gap energy value for GaN. Another finding refers to the transition energies appearing higher when the quaternary alloys constitute the barriers, when compared with the case in which InGaN is in the barriers. This can be explained by the effective mass values which are higher in the $\text{Al}_x\text{Ga}_y\text{In}_{1-x-y}\text{N}$ alloys than in InGaN.

It is also very important to investigate the influence of an external electrical field on the transition energies and how the results compare with those for the wurtzite phase structures. In Fig. 4, the theoretical PL and electroluminescence (EL) spectra were depicted at $T = 2$ K calculated for strained undoped $\text{In}_{0.1}\text{Ga}_{0.9}\text{N}/\text{Al}_x\text{Ga}_y\text{In}_{1-x-y}\text{N}$ SLs with $x=0.03, 0.10$ and 0.20 , and $y=0.50$. For these calculations the barrier width is $d_1 = 8$ nm and the well width is $d_2 = 3$ nm. The magnitude of the electric field was 1.6 MV/cm for the EL spectra calculations. The results indicate that the electric field enhances the shift seen in the spectra towards the red region, as compared with the PL spectra. This fact can be better visualized in Fig. 5, which shows the reduction in the transition energy as the electric field increases. Such behavior is attributed to the fact that the potentials become deeper as the electrical field increases. The main consequence is the presence of more levels occupied near the bottom of the potential wells. Comparing with wurtzite structures, which have intrinsic built-in electric fields, the situation described here is very similar, however in cubic systems higher efficiencies are predicted (Rodrigues et al. (2005)).

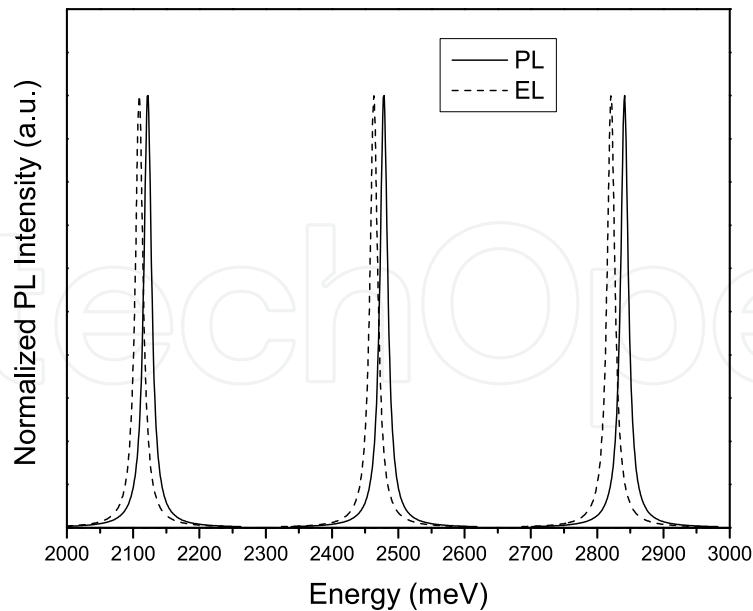


Fig. 4. Theoretical normalized PL (solid line) and electroluminescence (dashed line) spectra for strained undoped $\text{In}_{0.1}\text{Ga}_{0.9}\text{N}/\text{Al}_x\text{Ga}_y\text{In}_{1-x-y}\text{N}$ SLs, with $x = 0.03, 0.10,$ and $0.20,$ and $y = 0.50,$ respectively, barrier width $d_1 = 8$ nm and well width $d_2 = 3$ nm. The electric field used for EL was 1.6 MV/cm.

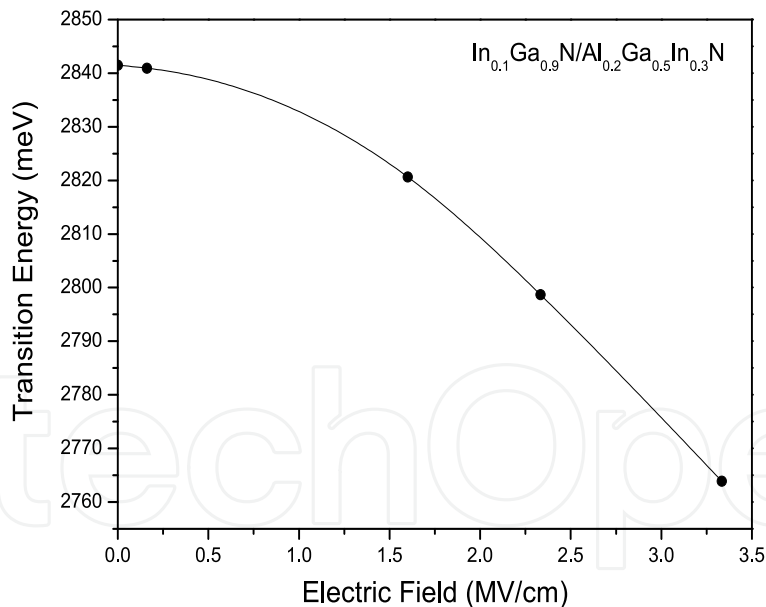


Fig. 5. PL peaks as a function of the magnitude of the electric field for systems with the same quaternary alloy contents as the ones in Fig. 4.

4. Doped cubic $\text{Al}_x\text{In}_y\text{Ga}_{1-x-y}\text{N}$ systems

An important aspect to be analyzed is the effect of the acceptor doping on the electronic transitions. Fig. 6 presents the PL spectra at $T = 2$ K for strained p-type doped $\text{Al}_{0.20}\text{Ga}_{0.05}\text{In}_{0.75}\text{N}/\text{Al}_x\text{In}_y\text{Ga}_{1-x-y}\text{N}$ SLs, for which x and y are varied as described in Table

2. The ionized acceptor doping concentration considered to be uniformly distributed in the barriers and fully ionized, is also varied assuming values of $N_A = 5 \times 10^{18} \text{cm}^{-3}$ and $N_A = 10 \times 10^{18} \text{cm}^{-3}$. These values of N_A allow us to envisage what happens in the range from very low hole concentrations up to concentrations as high as $\approx 10^{19} \text{cm}^{-3}$. The undoped system is also presented for comparison. The barriers widths are 8 nm and the wells widths are 3 nm (Rodrigues et al. (2007)). The choice of values for x and y , the Al and In alloy contents was such to reach all the visible-UV wavelength region.

c-(Al _{0.20} In _{0.05} Ga _{0.75})N/(Al _{<i>x</i>} In _{1-<i>x-y</i>} Ga _{<i>y</i>})N	<i>x</i>	<i>y</i>	1 - <i>x</i> - <i>y</i>
red	0.00	0.35	0.65
green	0.02	0.40	0.58
blue	0.08	0.45	0.47
blue-violet	0.10	0.50	0.40
violet	0.15	0.55	0.30

Table 2. Values used for the alloy contents x and y in the p -doped c-(Al_{0.20}In_{0.05}Ga_{0.75})N/(Al_{*x*}In_{1-*x-y*}Ga_{*y*})N SLs, properly chosen to attain light emission in the electromagnetic spectral regions indicated in the left column.

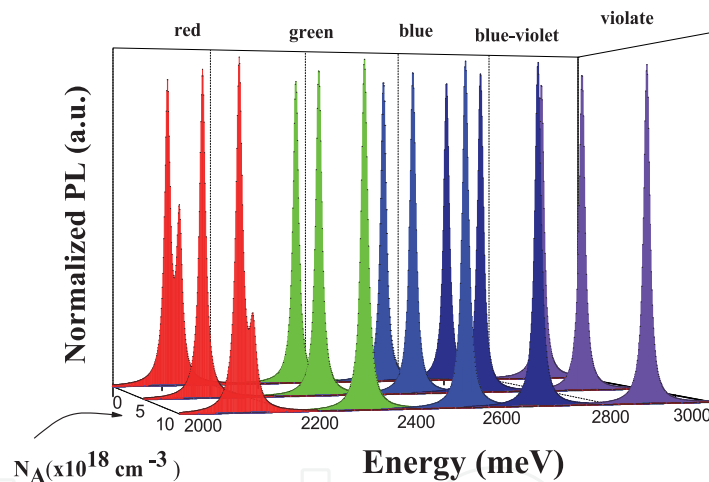


Fig. 6. Calculated normalized photoluminescence (PL) spectra, at $T = 2 \text{ K}$, for Al_{0.20}In_{0.05}Ga_{0.75}N/Al_{*x*}In_{1-*x-y*}Ga_{*y*}N SLs, for x and y values as shown in Table 2, for ionized acceptor concentrations of $N_A = 0$, $N_A = 5 \times 10^{18} \text{cm}^{-3}$, and $N_A = 10 \times 10^{18} \text{cm}^{-3}$. The energy range covers the electromagnetic spectrum from red to violet.

In Fig. 7 the PL peaks are depicted as a function of the acceptor doping concentration for the first electronic transition E1-HH1. As N_A increases a red-shift in energy is observed for all regions investigated, except for the red region which presents a second electronic transition E1-HH2 (first electron level E1 and second occupied heavy-hole level HH2) for $N_A = 0$ and $5 \times 10^{18} \text{cm}^{-3}$. This behavior is directly related to the transition probabilities in such systems and the potential profile due to the charges distribution. The later is determined by the balance between the Coulomb and exchange-correlation potentials contribution which defines the potential bending.

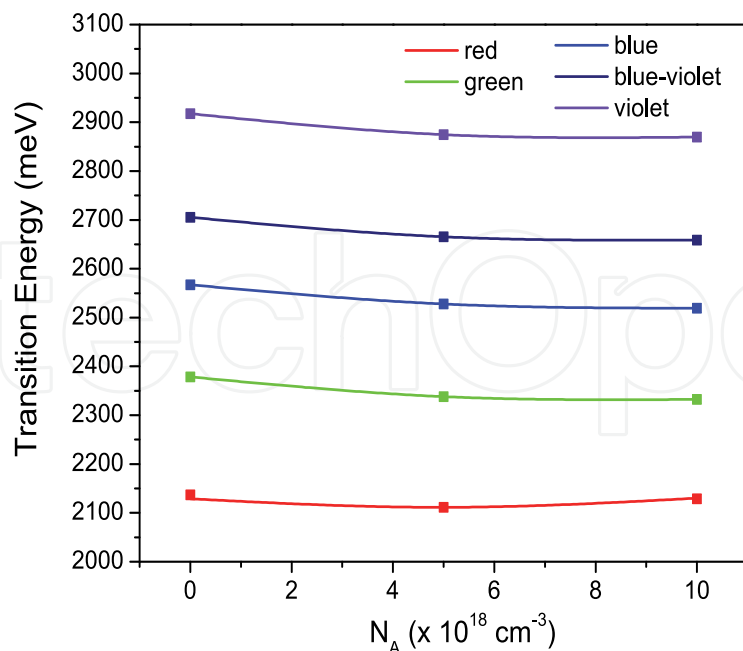


Fig. 7. Peaks of PL spectra of Fig. 6 as a function of the acceptor doping concentration, N_A .

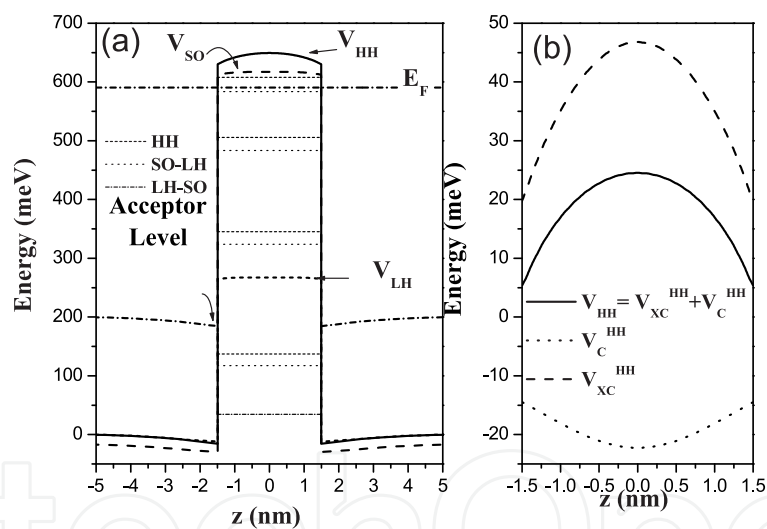


Fig. 8. p-doped $\text{Al}_{0.20}\text{In}_{0.05}\text{Ga}_{0.75}\text{N}/\text{In}_{0.65}\text{Ga}_{0.35}\text{N}$ SL, with $N_A = 5 \times 10^{18} \text{ cm}^{-3}$, which emits in the red: (a) Real-space energy diagram showing the spatial dependence of the valence band edges for heavy (V_{hh}), light (V_{lh}), and split-off (V_{so}) hole bands. Eight energy hole levels inside the well are depicted. Also shown, by thick dash-dotted lines, are the acceptor level in the barrier and the position of the Fermi level, E_F . The energy zero was taken at the top of the Coulomb potential at the barrier; (b) Different contributions to the self-consistent total heavy-hole potential (V_{hh}), due to the Coulomb (V_C^{hh}) and due to the exchange-correlation (V_{XC}^{hh}) potentials.

In order to enhance the visualization of this behavior, Fig. 8 shows (a) the potential profile for the $\text{Al}_{0.20}\text{In}_{0.05}\text{Ga}_{0.75}\text{N}/(\text{In}_{0.65}\text{Ga}_{0.35}\text{N})$ SL, with $N_A = 5 \times 10^{18} \text{ cm}^{-3}$, corresponding to the red emission in PL depicted in Fig. 7. The potential profile for each kind of carrier:

heavy-holes, V_{hh} , light-holes V_{lh} and split-off holes, V_{so} is shown, as well as the Fermi energy, E_F . The acceptor level is also indicated; for the nitrides, the acceptor level energy is deep, around 200 meV. However, the barriers in the nitrides are high since the strain effects are strong due the large lattice mismatch. The energy zero was placed at the top of the total Coulomb potential at the barrier. Fig. 8 (b) presents the exchange-correlation (V_{XC}^{hh}) and Coulomb potential (V_C^{hh}) profiles inside the well for the heavy-holes. For this case, in particular, the exchange-correlation potential stands out the Coulomb potential. So the total heavy-holes potential, V_{hh} is attractive and follows the same behavior of V_{XC} .

The rapid screening of the Coulomb potential because of the higher effective masses of the nitrides is responsible for this behavior. Consequently, the electronic transition decreases and the energy shifts to the red region.

The PL spectra behavior with the increase of the temperature could also be analyzed. Fig. 9 presents the PL spectra of one of the systems shown in Fig. 6, emitting in the red wavelength, the $\text{Al}_{0.20}\text{In}_{0.05}\text{Ga}_{0.75}\text{N}/\text{In}_{0.35}\text{Ga}_{0.65}\text{N}$ SL, with $N_A = 10 \times 10^{18} \text{ cm}^{-3}$. As seen above, at $T = 2$ K one can observe two peaks, E1-HH1 and E1-HH2. As the temperature increases, a red-shift in energy is seen. Above $T = 200$ K, other electronic transitions start to appear, showing a third peak (E1-HH3), and for $T = 300$ K, also a fourth peak (E1-HH4). This behavior is due to the higher probability of occupation of higher valence band energy levels as the temperatures increases. The red-shift in energy is a consequence of the band gap shrinkage. One can also observe that the peaks corresponding to the higher electronic transitions seen at $T = 200$ and 300 K are stronger due to the larger values for the oscillator strengths.

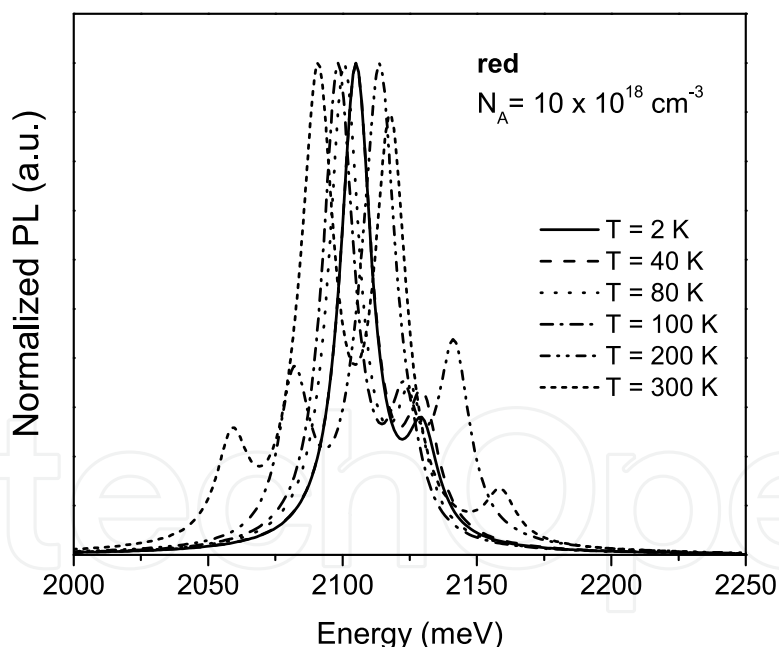


Fig. 9. Calculated PL spectra at $T = 2$ K (solid line), $T = 40$ K (dashed line), $T = 80$ K (dotted line), $T = 100$ K (dash-dotted line), $T = 200$ K (dash-dot-dotted line) and $T = 300$ K (short-dashed line) for the $\text{Al}_{0.20}\text{In}_{0.05}\text{Ga}_{0.75}\text{N}/\text{In}_{0.35}\text{Ga}_{0.65}\text{N}$ SL, with $N_A = 10 \times 10^{18} \text{ cm}^{-3}$, which emits in the red wavelength (see table 2).

Another important element to analyze in doped systems is the PL spectra dependence on the doping concentration. Fig. 10 depicts the calculated PL and absorption spectra, at $T = 2$ K, for a p -doped $\text{Al}_{0.20}\text{In}_{0.05}\text{Ga}_{0.75}\text{N}/\text{Al}_x\text{In}_{1-x-y}\text{Ga}_y\text{N}$ SL, corresponding to emission in the

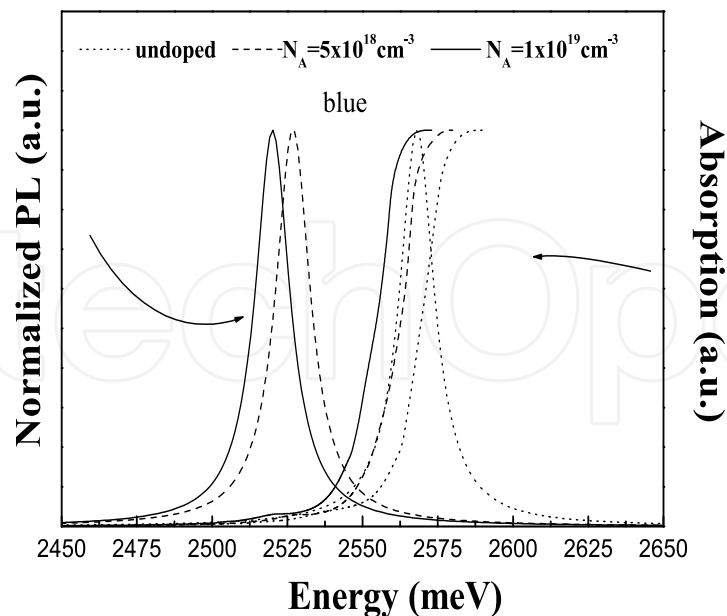


Fig. 10. Calculated PL and absorption spectra, at $T = 2$ K, for a p -doped $(\text{Al}_{0.20}\text{In}_{0.05}\text{Ga}_{0.75})\text{N}/(\text{Al}_x\text{In}_{1-x-y}\text{Ga}_y)\text{N}$ SL, which emits in the *blue* region (see Table II), for $N_A = 0$ (undoped), $N_A = 5 \times 10^{18} \text{cm}^{-3}$, and $N_A = 1 \times 10^{19} \text{cm}^{-3}$.

blue region, for $N_A = 0$ (undoped), $N_A = 5 \times 10^{18} \text{cm}^{-3}$, and $N_A = 10 \times 10^{18} \text{cm}^{-3}$. One can clearly observe a red shift in both, the PL and absorption spectra, as the acceptor doping concentration increases due to the confinement and many body effects. From these results the values obtained for the Stokes shift can be extracted, taken as the energy difference between the PL peak and the absorption edge. A significant increasing in the values of the Stokes shifts with the increase of N_A can be seen. This is due to the fact that many-body effects such as exchange and correlation within the 2DHG have shown to be relevant, particularly for high hole-density systems. The values encountered for the Stokes shifts in the systems shown in Fig. 10 are approximately 20 meV and 40 meV, respectively, for $N_A = 5 \times 10^{18} \text{cm}^{-3}$ and $N_A = 10 \times 10^{18} \text{cm}^{-3}$. Similar values for the Stokes shifts have been found for p -doped ternary $(\text{AlGa})\text{N}/\text{GaN}$ SLs (Rodrigues et al. (2007)).

5. Double $\text{Al}_x\text{In}_y\text{Ga}_{1-x-y}\text{N}$ quantum wells

This section is dedicated to the study of the PL spectra for undoped and p -doped $\text{Al}_x\text{In}_{1-x-y}\text{Ga}_y\text{N}/\text{Al}_x\text{In}_{1-x-y}\text{Ga}_y\text{N}$ double quantum wells (DQWs), in which the Al and the In contents, as well as, the well and spike widths are varied. A schematic diagram of the investigated DQWs is presented in Fig. 11. The well and spike widths, d_w and d_s , respectively, are indicated. The first electronic transition is also shown and corresponds to the transition between the first electron level and the first occupied heavy-hole level (E1- HH1) (Rodrigues et al. (2008)).

Fig. 12 presents the theoretical PL spectra from undoped DQWs constituted by $\text{Al}_{0.25}\text{In}_{0.05}\text{Ga}_{0.70}\text{N}$ in the barrier, 10 nm width, followed by a variable width well (d_w) of $\text{Al}_{0.08}\text{In}_{0.37}\text{Ga}_{0.55}\text{N}$, a variable width spike (d_s) of $\text{Al}_{0.10}\text{In}_{0.10}\text{Ga}_{0.80}\text{N}$, again a variable width well (d_w) of $\text{Al}_{0.08}\text{In}_{0.37}\text{Ga}_{0.55}\text{N}$ and a fixed barrier of 10 nm of $\text{Al}_{0.25}\text{In}_{0.05}\text{Ga}_{0.70}\text{N}$. This set of spectra corresponds to the cases in which the spike width is fixed in 4 nm and the well width is varied

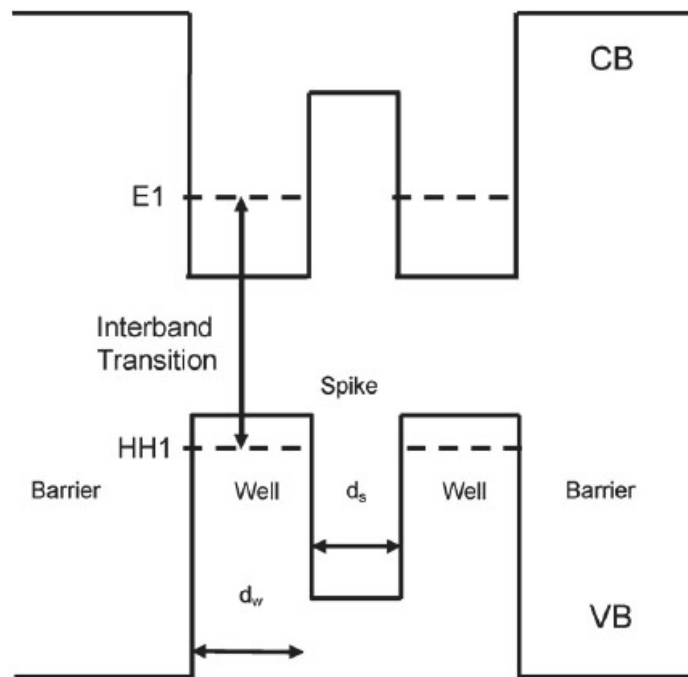


Fig. 11. Schematic diagram for the conduction and valence bands of the DQW structure investigated here. d_w and d_s are the well and the spike widths, respectively. The interband transition is also indicated, as well as the first electron (E1) and heavy-hole (HH1) occupied levels.

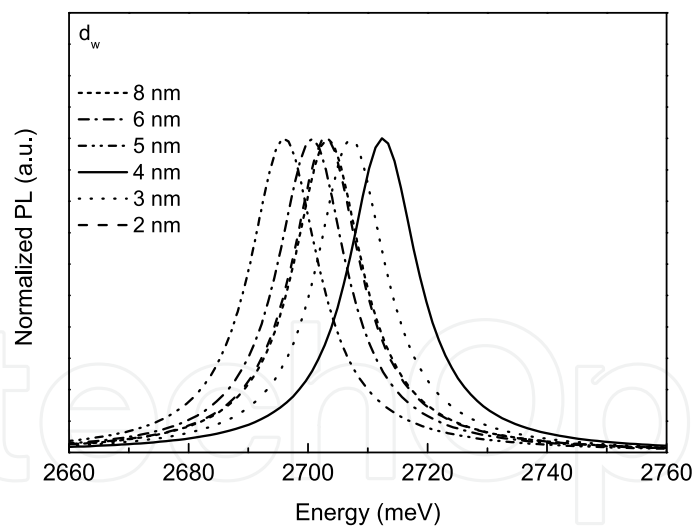


Fig. 12. Calculated PL spectra at $T = 2$ K for undoped $c\text{-Al}_{0.25}\text{In}_{0.05}\text{Ga}_{0.70}\text{N}/\text{Al}_{0.08}\text{In}_{0.37}\text{Ga}_{0.55}\text{N}/\text{Al}_{0.10}\text{In}_{0.10}\text{Ga}_{0.80}\text{N}$ DQWs for well width $d_w = 4$ nm and spike widths $d_s = 8$ nm, 6 nm, 5 nm, 4 nm, 3 nm, and 2 nm.

from 2 nm, 3 nm, 4 nm, 5 nm, 6 nm, to 8 nm. A blue-shift is present in energies up to $d_w = 4$ nm, whereas there is a red-shift for $d_w > 4$ nm, and beyond this value a blue-shift is observed for values of $d_w > 5$ nm. This behavior can be explained by the fact that for $d_w < 4$ nm the DQW is in an interacting regime and at $d_w = 5$ nm it reaches the changing point from interacting

regime to isolated QWs. For larger wells, the spike width loses its importance and above $d_w = 5$ nm it occurs a blue-shift in the energy due to the confinement effects for isolated wells.

Fig. 13 presents calculated PL spectra for systems with fixed well width $d_w = 4$ nm and spike width, d_s , varying from 2 to 8 nm. One can observe a red-shift in energy as d_s increases. This leads to the conclusion that confinement levels are localized deeper, decreasing the electronic transition energies.

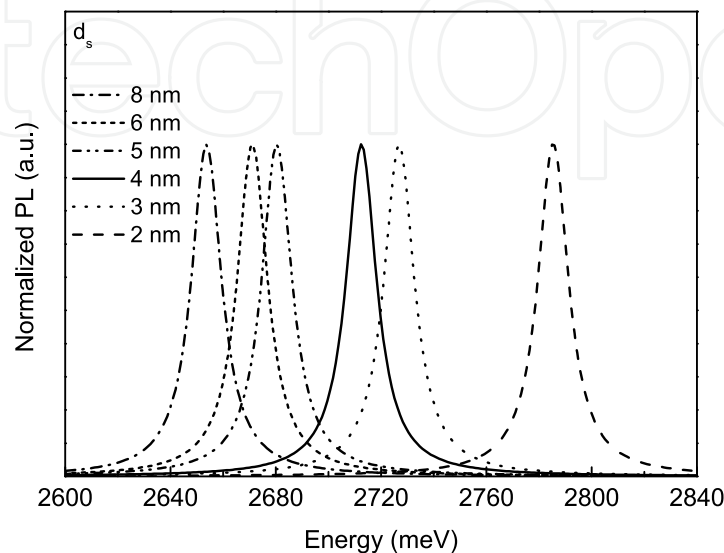


Fig. 13. Calculated PL spectra at $T = 2$ K for undoped $c\text{-Al}_{0.25}\text{In}_{0.05}\text{Ga}_{0.70}\text{N}/\text{Al}_{0.08}\text{In}_{0.37}\text{Ga}_{0.55}\text{N}/\text{Al}_{0.10}\text{In}_{0.10}\text{Ga}_{0.80}\text{N}$ DQWs for the spike width $d_s = 4$ nm and well width $d_w = 8$ nm, 6 nm, 5 nm, 4 nm, 3 nm, and 2 nm.

To analyze the properties of doped systems, Fig. 14 presents the PL spectra at 2 K for the same system depicted in Fig. 12, and for spike and well widths fixed at 4 nm. The two-dimensional (2D) acceptor doping concentration is varied assuming values of $N_{2D} = 2 \times 10^{12} \text{cm}^{-2}$, $4 \times 10^{12} \text{cm}^{-2}$, and $8 \times 10^{12} \text{cm}^{-2}$. The undoped system is also presented for comparison. One can observe a red-shift in energy up to $N_{2D} = 4 \times 10^{12} \text{cm}^{-2}$, and for $N_{2D} = 8 \times 10^{12} \text{cm}^{-2}$ a blue-shift is seen. This behavior is due to the potential profile, which shows a bending that curves up for low concentrations, and curves down for high concentrations, no matter whether the total potential is attractive or repulsive. An attractive potential is observed up to $4 \times 10^{12} \text{cm}^{-2}$, so the levels are localized near the bottom of the wells, beyond that, the potential is repulsive, and one can expect larger transition energies.

The last issue to be addressed in DQWs is the strain. Fig. 15 presents the PL spectra at $T = 2$ K for strained p-type doping $\text{Al}_{0.60}\text{In}_{0.05}\text{Ga}_{0.35}\text{N}/\text{Al}_{0.10}\text{In}_{0.40}\text{Ga}_{0.50}\text{N}/\text{In}_{0.10}\text{Ga}_{0.90}\text{N}$ DQWs, in order to analyze the spike effects. The two-dimensional acceptor donor concentration was fixed in $N_{2D} = 2 \times 10^{12} \text{cm}^{-2}$. Fig. 15(a) presents the spectra for a fixed spike width $d_s = 4$ nm and (b) for fixed well widths $d_w = 4$ nm. One can observe in Fig. 15 (a) a red-shift in energy due to confinement effects as d_s increases. This behavior is opposite to the one seen in Fig. 15 (b), where a blue-shift in energy exists until $d_w = 3$ nm, followed by a red shift, where a change from an interacting to an isolated well regime occurs. After $d_s = 5$ nm, again a blue-shift in energy is observed, due to many body effects, which become more important than the spike width contribution to these systems. It is important to note that a different behavior is observed if compared with undoped systems. This is related to the charge distribution

inside the wells, with the Fermi level lying near the bottom of wells for thicker wells, contrary to what is observed for thin ones. Note that in this case the transition from interacting to isolated regime occurs in $d_s = 4$ nm.

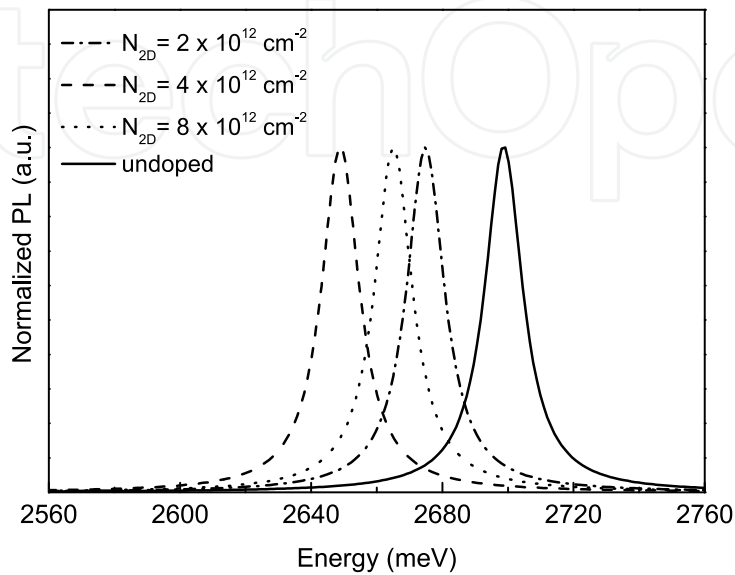
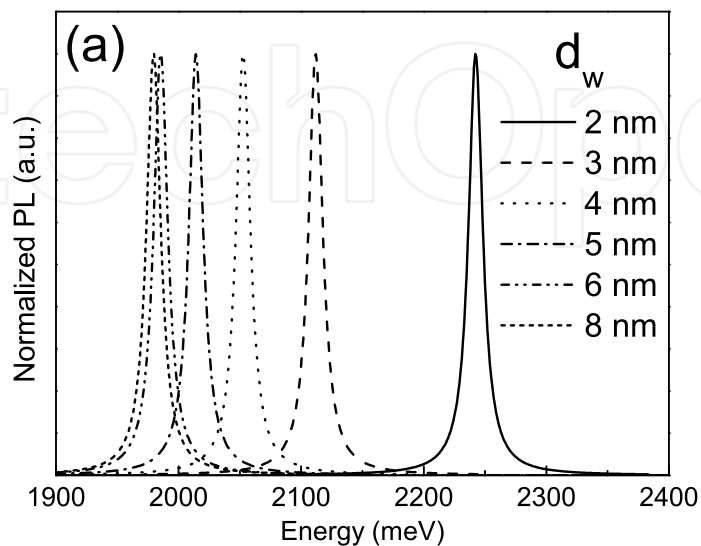


Fig. 14. Calculated PL spectra at $T = 2$ K for p -doped $c\text{-Al}_{0.25}\text{In}_{0.05}\text{Ga}_{0.70}\text{N}/\text{Al}_{0.08}\text{In}_{0.37}\text{Ga}_{0.55}\text{N}/\text{Al}_{0.10}\text{In}_{0.10}\text{Ga}_{0.80}\text{N}$ DQWs, for well and spike widths equal to 4 nm and doping $N_{2D} = 2 \times 10^{12} \text{ cm}^{-2}$ (dashed-dot line), $4 \times 10^{12} \text{ cm}^{-2}$ (dashed line), $8 \times 10^{12} \text{ cm}^{-2}$ (dotted line), and undoped (solid line) for comparison.



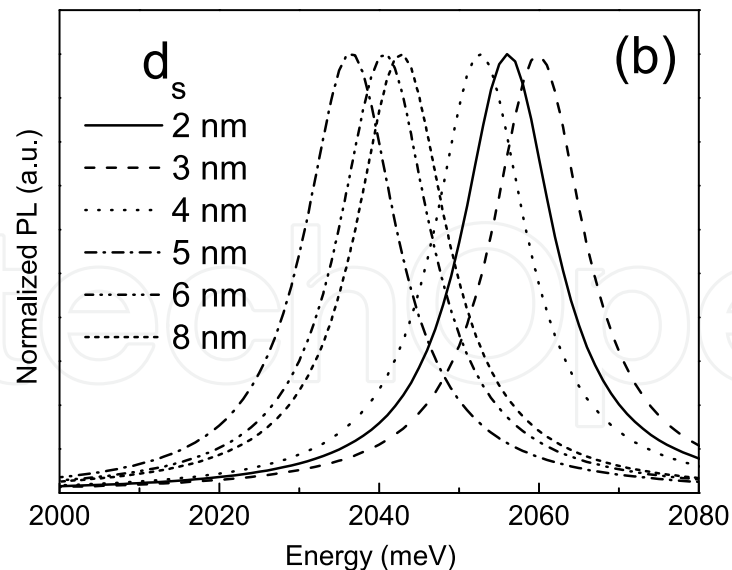


Fig. 15. Theoretical normalized PL spectra at 2 K for strained $c\text{-Al}_{0.60}\text{In}_{0.05}\text{Ga}_{0.35}\text{N}/\text{Al}_{0.10}\text{In}_{0.40}\text{Ga}_{0.50}\text{N}/\text{In}_{0.10}\text{Ga}_{0.90}\text{N}$ DQWs, fully p-doped barrier with $N_{2D} = 2 \times 10^{12} \text{cm}^{-2}$. The systems have (a) fixed $d_s = 4 \text{ nm}$ and varying from $d_w = 2 \text{ nm}$ to 8 nm , and (b) fixed $d_w = 4 \text{ nm}$ and varying from $d_s = 2 \text{ nm}$ to 8 nm .

6. Conclusions

In this chapter it was performed a detailed investigation of the theoretical luminescence and absorption spectra of strained undoped and doped $c\text{-Al}_x\text{In}_{1-x-y}\text{Ga}_y\text{N}/\text{Al}_x\text{In}_{1-x-y}\text{Ga}_y\text{N}$ SLs and DQWs using a self-consistent resolution of the 8×8 Kane Hamiltonian within the effective mass theory.

At first it was shown the feasibility of reaching emissions from red light to blue light regions by the correct combination of different quaternary alloys either in the well or in the barrier in undoped systems. When an external field is taken into account, the theoretical spectra present red shifts. A similar result could be obtained for the wurtzite phase of the structures, caused by the presence of the intrinsic piezoelectric fields. In such systems, these effects lead to a spatial segregation of the electron and hole charge distributions, causing a reduction in the light emission efficiency. For the cubic phase structures, as the piezoelectric fields are absent, the spatial segregation is smaller and therefore higher efficiency would be expected.

Analyzing the doped systems, it is pointed out that light emission arising from the recombination involving confined states in the wells has not a monotonic behavior when the doping concentration increases, even if it is always red shifted when compared to the undoped SLs. The main reason for this is the shape of the potential bending induced by the presence of a holes charge distribution inside the wells. The competition between the exchange-correlation potential and the Coulomb potential was shown to be the main reason for this behavior, since they define the total bending potential, attractive or repulsive, which affects directly the optical transitions. Again, for single QWs, it was shown that by choosing an appropriate set of alloy molar fractions and acceptor concentrations it is possible to achieve white light emission by combining the emission in three different regions of the spectra.

Regarding to different spatial arrangements, DQWs were analyzed. It was shown for p-doped $c\text{-Al}_x\text{In}_{1-x-y}\text{Ga}_y\text{N}/\text{Al}_x\text{In}_{1-x-y}\text{Ga}_y\text{N}$ DQWs that the related PL spectra depict a different behavior depending on the spike and/or adjacent well layer widths. A change in the kind of regime from interacting wells to isolated non-interacting wells was demonstrated. Although not shown here, it is also possible to reach all wavelengths using the DQWs structures, as it was demonstrated for single QWs.

Another important conclusion that must be pointed out from the set of systems analyzed in the chapter is that the red region of electromagnetic spectrum can be reached through the quaternary alloys using less In content, as compared to the ternary InGaN alloy. From the experimental point of view this finding is fundamental, since the growth with higher In content is more difficult.

Finally, supported by the recent advances in the growth techniques, the analysis presented here intends to elucidate and guide the study of optical properties in semiconductor nitride systems, bringing new possibilities for experiments and, hopefully, novel proposals for the next generation of advanced optical devices.

7. Acknowledgments

The authors thank O. F. P. dos Santos of the Universidade Federal Rural de Pernambuco for the discussions and Prof. E. L. Piner of Texas State University for his suggestions. We also express our thanks to the support received from the Brazilian research financial agencies CNPq (grants nos 564.739/2010-3/NanoSemiCon, 303.880/2008-2/PQ, 470.998/2010-5/Univ, 472.312/2009-0/Univ 304936/2009-0/ PQ, 303578/ 2007-6/ PQ, 577.219/2008-1/JP), CAPES, FACEPE (grant no. 0553-1.05/10/APQ), and FAPESP. LS also acknowledges partial support from the Materials Science, Engineering and Commercialization Program of Texas State University.

8. References

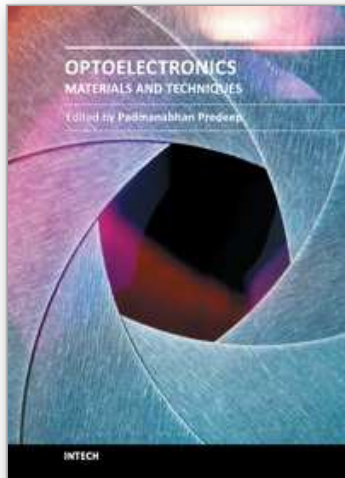
- Ambacher, O. (1998). Growth and applications of Group III-nitrides. *Journal of Physics D: Applied Physics*, Vol. 31, No. 20, (October 1998) pp. 2653- 2710, ISSN 1361-6463
- As, D. J. (2009). Cubic group-III nitride-based nanostructures basics and applications in optoelectronics. *Microelectronics Journal*, Vol. 40, No. 2, (September 2008) pp. 204- 209, ISSN 0022-0248
- Enderlein, R.; Sipahi, G.; Scolfaro, L. M. R. & Leite, J. R. (1997). Density functional theory for holes in semiconductors. *Physical Review Letters*, Vol. 79, No. 19, (November 1997) pp. 3712-3715, ISSN 0031-9007
- Fernández-Garrido, S.; Redondo-Cubero, A.; Gago, R.; Bertram, F.; Luna, E.; Trampert, A.; Pereiro, J.; Muñoz, E. & Calleja, E. (2008). Effect of the growth temperature and the AlN mole fraction on In incorporation and properties of quaternary III-nitride layers grown by molecular beam epitaxy. *Journal Applied Physics*, Vol. 104, No. 8, (October 2010) pp. 083510-1 -083510-7, ISSN 0021-8979
- Fu, Y-K.; Jiang, R-H.; Lu, Y-H.; Chen, B-C.; Xuan, R.; Fang, Y-H.; Lin, C-F.; Su, Y-K. & Chen, J-F. (2011). The effect of trimethylgallium flows in the AlInGaN barrier on optoelectronic characteristics of near ultraviolet light-emitting diodes grown by atmospheric pressure metalorganic vapor phase epitaxy. *Applied Physics Letters*, Vol. 98, No. 12, (March 2011) pp. 121115-1 -121115-3, ISSN 0003-6951

- Hirayama, H. (2005). Quaternary InAlGaN-based high-efficiency ultraviolet light-emitting diodes. *Journal of Applied Physics*, Vol. 97, No. 9, (April 2005) pp. 091101-1-091101-19, ISSN 0021-8979
- Hirayama, H.; Noguchi, N. & Kamata, N. (2010). 222nm Deep-Ultraviolet AlGaIn Quantum Well Light-Emitting Diode with Vertical Emission Properties. *Applied Physics Express*, Vol. 3, No. 3, (March 2010) pp. 032102-1-032102-3, ISSN 1882-0778
- Kemper, R. M.; Weigl, M.; Mietze, C.; Härbelen, M. H.; Schupp, T.; Tshucmak, E.; Lindner, J. K. N., Lischka, K. & As, D. J. (2011). Growth of cubic GaN on nano-patterned 3C-SiC/Si(001) substrates. *Journal Crystal Growth*, Vol. 323, No. 1, (May 2011) pp. 84-87, ISSN 0022-0248
- Kim, K. H.; Li, S.; Jin, S. X.; Lin, J. Y. & Jianga, H. X. (2003). III-nitride ultraviolet light-emitting diodes with delta doping. *Applied Physics Letters*, Vol. 83, No. 3, (July 2003) pp. 566-568, ISSN 0003-6951
- Knauer, A.; Wenzel, H.; Kolbe, T.; Einfeldt, S.; Weyers, M.; Kneissl, M. & Tränkle, G. (2008). Effect of the barrier composition on the polarization fields in near UV InGaIn light emitting diodes. *Applied Physics Letters*, Vol. 92, No. 19, (May 2008) pp. 191912-1-191912-3, ISSN 0003-6951
- Kyono, T.; Hirayama, H.; Akita, K.; Nakamura, T.; Adachi, M. & Ando, K. (2006). Influence of residual oxygen impurity in quaternary InAlGaIn multiple-quantum-well active layers on emission efficiency of ultraviolet light-emitting diodes on GaN substrates. *Journal Applied Physics*, Vol. 99, No. 11, (June 2006) pp. 114509-1-114509-7, ISSN 0021-8979
- Kohler, U.; As, D. J.; Potthast, S.; Khartchenko, A.; Lischka, K.; Noriega, O. C.; Meneses, E. A.; Tabata, A.; Rodrigues, S. C. P.; Scolfaro, L. M. R.; Sipahi, G. M. & Leite, J. R. (2002). Optical Characterization of Cubic AlGaIn/GaN Quantum Wells. *physica statu solid (a)*, Vol. 192, No. 1, (July 2002) pp. 129-134, ISSN 1862-6319
- Liu, J.; Zhang, Y.; Lochner, Z.; Kim, S-S.; Kim, H-S.; Ryou, J-H.; Shen, S-C.; Yoder, P. D.; Dupuis, R. D.; Wei, Q. Y.; Sun, K. W.; Fisher, A. M. & Ponce, F. A. (2011). Performance characteristics of InAlGaIn laser diodes depending on electron blocking layer and wave guiding layer design grown by metalorganic chemical vapor deposition. *Journal of Crystal Growth*, Vol. 315, No. 1, (October 2010) pp. 272-277, ISSN 0021-8979
- Marques, M.; Teles, L. K.; Scolfaro, L. M. R.; Leite, J. R.; Furthmüller, J. & Bechstedt, F. (2003). Lattice parameter and energy band gap of cubic $\text{Al}_x\text{Ga}_y\text{In}_{1-x-y}\text{N}$ quaternary alloys. *Applied Physics Letters*, Vol. 83, No. 5, (March 2003) pp. 890-893, ISSN 0003-6951
- Nakamura, S.; Senoh, M.; Iwasa, N. & Nagahama, S. (1995). High-power InGaIn single-quantum-well-structure blue and violet light-emitting diodes. *Applied Physics Letters*, Vol. 67, No. 13, (July 1995) pp. 1868-1870, ISSN 0003-6951
- Nakamura, S.; Pearton, S. & Fasol, G. (2000). *The Blue Laser Diode: the complete story*, Springer, ISBN 3-540-66505-6, Berlin.
- Park, S-H; Ahn, D. & Kim, J-W. (2008). Optical gain in InGaIn/InGaAlN quantum well structures with zero internal field. *Applied Physics Letters*, Vol. 92, No. 17, (May 2008) pp. 171115-1-171115-3, ISSN 0003-6951
- Ramos, L. E.; Teles, L. K.; Scolfaro, L. M. R.; Castineira, J. L. P.; Rosa, A. L. & Leite, J.R. (2001). Structural, electronic, and effective-mass properties of silicon and zinc-blende group-III nitride semiconductor compounds. *Physical Review B*, Vol. 63, No. 16, (April 2001) pp. 165210-1-165210-10, ISSN 1098-0121

- Roberts, J. C.; McIntosh, F. G.; Aumer, M. E.; Piner, E. L.; Joshkin, V. A.; Liu, S.; El-Masry, N. A. & Bedair, S. M. (1996). Stacked InGaN/AlGaN Double Heterostructures. *1996 MRS Proceedings*, Vol. 449, No. 1, (December 1996) pp. 1161-1165, ISSN 1946-4274
- Rodrigues, S. C. P.; Scolfaro, L. M. R.; Leite, J. R. & Sipahi, G. M. (2000). Valence band structure of cubic AlGaN/GaN superlattices. *Applied Physics Letters*, Vol. 76, No. 8, (December 1999) pp. 1015-1017, ISSN 0003-6951
- Rodrigues, S. C. P.; Sipahi, G.; Scolfaro, L. M. R. & Leite, J. R. (2001). Exchange-correlation effects on the hole miniband structure and confinement potential in zincblende AlGaN/GaN superlattices. *Journal of Physics. Condensed Matter*, Vol. 13, No. 14, (April 2001) pp. 3381-3387, ISSN 0953-8984
- Rodrigues, S. C. P.; Sipahi, G.; Scolfaro, L. M. R. & Leite, J. R. (2002). Hole charge localization and band structures of p-doped GaN/InGaN and GaAs/InGaAs semiconductor heterostructures. *Journal of Physics. Condensed Matter*, Vol. 14, No. 23, (May 2002) pp. 5813-5827, ISSN 0953-8984
- Rodrigues, S. C. P.; Sipahi, G. M. & da Silva Jr, E. F. (2005). Optical and electronic properties of AlInGaN/InGaN superlattices. *Microelectronics Journal* *Microelectronics Journal*, Vol. 36, No. 3-6, (March 2005) pp. 434-437, ISSN 0022-0248
- Rodrigues, S. C. P.; d'Eurydice, M. N.; Sipahi, G. M. & da Silva Jr, E. F. (2005). Design of InGaN/AlInGaN superlattices for white-light device applications. *Microelectronics Journal*, Vol. 36, No. 3-6, (March 2005) pp. 1002-1005, ISSN 0022-0248
- Rodrigues, S. C. P.; d'Eurydice, M. N.; Sipahi, G. M.; Scolfaro, L. M. R. & da Silva Jr, E. F. (2007). White light emission from p-doped quaternary (InGaAl)N-based superlattices: theoretical calculations for the cubic phase. *Journal Applied Physics*, Vol. 101, No. 11, (June 2007) pp. 113706-113706-6, ISSN 0021-8979
- Rodrigues, S. C. P.; dos Santos, O. F. P.; Scolfaro, L. M. R.; Sipahi, G. M. & da Silva Jr, E. F. (2008). Luminescence Studies on Nitride Quaternary Alloys Double Quantum Wells. *Applied Surface Science*, Vol. 254, No. 23, (February 2008) pp. 7790-7793, ISSN 0169-4332
- Schörmann, J.; As, D. J.; Lischka, K.; Schley, P.; Goldhahn, R.; Li, S. F.; Lffler, W.; Hetterich, M. & Kalt, H. (2006). Molecular beam epitaxy of phase pure cubic InN. *Applied Physics Letters*, Vol. 89, No. 26, (December 2006) pp. 261903-261905, ISSN 0003-6951
- Schörmann, J.; Potthast, S.; As, D. J. & Lischka, K. (2007). Molecular beam epitaxy of phase pure cubic InN. *Applied Physics Letters*, Vol. 90, No. 4, (January 2007) pp. 041918-1-041918-3, ISSN 0003-6951
- Scolfaro, L. M. R.; Teles, L. K.; Marques, M.; Ferreira, L. G. & Leite, J. R. (2004). Phase Separation and Ordering in Cubic Ternary and Quaternary Nitride Alloys, In: *Optoelectronic Devices: III-Nitrides*, M. Razegui, M. Henini, (Ed.), pp. 455-478, Elsevier, ISBN 0-08-044426-1, Oxford
- Sipahi, G. M.; Enderlein, R.; Scolfaro, L. M. R. & Leite, J. R. (1996). Band structure of holes in p-type δ -doping quantum wells and superlattices. *Physical Review B*, Vol. 53, No. 15, (april 1996) pp. 9930-9942, ISSN 1098-0121
- Sipahi, G. M.; Enderlein, R.; Scolfaro, L. M. R.; Leite, J. R. & Levine, A. (1998). Theory of luminescence spectra from δ -doping structures: application to GaAs. *Physical Review B*, Vol. 57, No., (April 1998) pp. 9168-9178, ISSN 1098-0121
- Suihkonen, S.; Svensk, O.; Törmä, P. T.; Ali, M.; Sopane, M.; Lipsanen, H.; Odnoblyudo, M. A. & Bougrov, V. E. (2008). MOVPE growth and characterization of InAlGaN films and InGaN/InAlGaN MQW structures. *Journal of Crystal Growth*, Vol. 310, No. 7-9, (November 2007) pp. 1777-1780, ISSN 0022-0248

- Tabata, A.; Teles, L. K.; Scolfaro, L. M. R.; Leite, J. R.; Frey, T.; Kharchenko, A.; As, D. J.; Schikora, D.; Lischka, K.; Furthmüller, J. & Bechstedt, F. (2002). Phase separation suppression in InGaN epitaxial layers due to biaxial strain. *Applied Physics Letters*, Vol. 80, No. 5, (November 2001) pp. 769-771, ISSN 0003-6951
- Tschumak, E.; Granzner, R.; Lindner, J. K. N.; Schwierz, F.; Lischka, K.; Nagasawa, H.; Abe, M. & As, D. J. (2008). Nonpolar cubic AlGaIn/GaN heterojunction field-effect transistor on Ar⁺ implanted 3C-SiC (001). *Applied Physics Letters*, Vol. 96, No. 25, (June 2010) pp. 253501-1 - 253501-3, ISSN 0003-6951
- Xiao D.; Kim, K. W.; Bedair, S. M. & Zavada, J. M. (2004). Design of white light-emitting diodes using InGaIn/AlInGaIn quantum-well structures. *Applied Physics Letters*, Vol. 84, No. 5, (February 2004) pp. 672-674, ISSN 0003-6951
- Xie, J.; Leach, J. H.; Ni, X.; Wu, M.; Shimada, R.; Özgür, Ü. & Morkoç, H.; (2007). Electron mobility in InGaIn channel heterostructure field effect transistor structures with different barriers. *Applied Physics Letters*, Vol. 91, No. 26, (November 2007) pp. 262102-1 -262102-3, ISSN 0003-6951
- Zado, A.; Tschumak, E.; Gerlach, J. W.; Lischka, K. & As, D. J. (2011). Carbon as an acceptor in cubic GaN/3CSiC. *Journal of Crystal Growth*, Vol. 323, No. 1, (may 2011) pp. 88 -90, ISSN 0022-0248
- Zhmakin, A. I. (2011). Enhancement of light extraction from light emitting diodes *Physics Reports*, Vol. 498, No. 4-5, (November 2010) pp. 189-241, ISSN 0370-1573
- Zhang, L.; Ding, K.; Liu, N. X.; Wei, T. B.; Ji, X. L.; Ma, P.; Yan, J. C.; Wang, J. X.; Zeng, Y. P. & Li, J. M. (2011). Theoretical study of polarization-doped GaN-based light-emitting diodes. *Applied Physics Letters*, Vol. 98, No. 10, (March 2011) pp. 101110-1 -101110-3, ISSN 0003-6951
- Zhu, D.; Kappers, M. J.; McAleese, C.; Graham, D. M.; Chabrol, G. R.; Hylton, N.P.; Dawson, P.; Thrush, C. J. & Humphreys, C. J. (2007). Optical and micro-structural properties of high photoluminescence efficiency InGaIn/AlInGaIn quantum well structures. *Journal of Crystal Growth*, Vol. 298, No. 1, (November 2007) pp. 504 -507, ISSN 0022-0248
- Wang, F.; Li, S-S.; Xia, J-B.; Jiang, H. X.; Lin, J. Y.; Li, J. & Wei, S-H.; (2007). Effects of the wave function localization in AlInGaIn quaternary alloys. *Applied Physics Letters*, Vol. 91, No. 6, (August 2007) pp. 061125-1 - 061125-3, ISSN 0003-6951

IntechOpen



Optoelectronics - Materials and Techniques

Edited by Prof. P. Predeep

ISBN 978-953-307-276-0

Hard cover, 484 pages

Publisher InTech

Published online 26, September, 2011

Published in print edition September, 2011

Optoelectronics - Materials and Techniques is the first part of an edited anthology on the multifaceted areas of optoelectronics by a selected group of authors including promising novices to the experts in the field. Photonics and optoelectronics are making an impact multiple times the semiconductor revolution made on the quality of our life. In telecommunication, entertainment devices, computational techniques, clean energy harvesting, medical instrumentation, materials and device characterization and scores of other areas of R&D the science of optics and electronics get coupled by fine technology advances to make incredibly large strides. The technology of light has advanced to a stage where disciplines sans boundaries are finding it indispensable. Smart materials and devices are fast emerging and being tested and applications developed in an unimaginable pace and speed. Here has been made an attempt to capture some of the materials and techniques and underlying physical and technical phenomena that make such developments possible through some real time players in the field contributing their work and this is sure to make this collection of essays extremely useful to students and other stake holders such as researchers and materials scientists in the area of optoelectronics.

How to reference

In order to correctly reference this scholarly work, feel free to copy and paste the following:

Sara C. P. Rodrigues, Guilherme M. Sipahi, Luísa Scolfaro and Eronides F. da Silva Jr. (2011). Application of Quaternary AlInGaN- Based Alloys for Light Emission Devices, Optoelectronics - Materials and Techniques, Prof. P. Predeep (Ed.), ISBN: 978-953-307-276-0, InTech, Available from:
<http://www.intechopen.com/books/optoelectronics-materials-and-techniques/application-of-quaternary-alingan-based-alloys-for-light-emission-devices>

INTECH
open science | open minds

InTech Europe

University Campus STeP Ri
Slavka Krautzeka 83/A
51000 Rijeka, Croatia
Phone: +385 (51) 770 447
Fax: +385 (51) 686 166
www.intechopen.com

InTech China

Unit 405, Office Block, Hotel Equatorial Shanghai
No.65, Yan An Road (West), Shanghai, 200040, China
中国上海市延安西路65号上海国际贵都大饭店办公楼405单元
Phone: +86-21-62489820
Fax: +86-21-62489821

© 2011 The Author(s). Licensee IntechOpen. This chapter is distributed under the terms of the [Creative Commons Attribution-NonCommercial-ShareAlike-3.0 License](#), which permits use, distribution and reproduction for non-commercial purposes, provided the original is properly cited and derivative works building on this content are distributed under the same license.

IntechOpen

IntechOpen